Band structure engineering of van der Waals heterostructures using ferroelectric clamped sandwich structures

Hao Tian, Changsong Xu, Xu Li, Yurong Yang, L. Bellaiche, and Di Wu

Phys. Rev. B **103**, 125426 — Published 25 March 2021

DOI: 10.1103/PhysRevB.103.125426

Band structure engineering of van der Waals heterostructures using ferroelectric clamped sandwich structures

Hao Tian,[1,2] Changsong Xu,[3] Xu Li,[1,2] Yurong Yang,[1,2,*] L. Bellaiche,[3] and Di Wu[1,2,†]

[1] *National Laboratory of Solid State Microstructures and Collaborative Innovation Center of Advanced Microstructures, Department of Materials Science and Engineering, Nanjing University, Nanjing 210093, China*

[2] *Jiangsu Key Laboratory of Artificial Functional Materials, Nanjing University, Nanjing 210093, China*

[3] *Physics Department and Institute for Nanoscience and Engineering, University of Arkansas, Fayetteville, Arkansas 72701, USA*

(Dated: March 11, 2021)

A novel strategy of band structure engineering of van der Waals heterostructure is proposed using a ferroelectric clamped sandwich structure from first principles. The validity of the strategy is demonstrated in the sandwich structure of In_2Se_3/bilayer-CrI_3/In_2Se_3 (In_2Se_3/bi-CrI_3/In_2Se_3) made by ferroelectric (FE) In_2Se_3 layers and semiconducting bilayer (SB) CrI_3. Four states with different band structure in the FE/SB/FE sandwich structure are obtained by switching the ferroelectric polarization in the top and bottom In_2Se_3 layers. Two of the states possess spin-splitting semiconducting band structures with opposite spin channel in conduction bands which are generated from a spin degenerated band structure of the CrI_3 bilayer, resulting in an electric field controllable and non-volatile four states spin-field effect transistor. The strategy of using ferroelectric layers to engineer band structures and generate spin-splitting semiconducting band structure in van der Waals heterostructure opens a new route in 2D electronics and spintronics.

I. INTRODUCTION

Semiconducting heterostructures are the essential materials foundation for all modern electronics and optoelectronics. Integrating of heterostructures by dissimilar materials with pristine interface is the foundation of functional devices and has been long the pursuit of materials community. However, epitaxially growing heterostructures with dissimilar materials may easily generate interfacial disorder. Two-dimensional (2D) materials offer a unique opportunity for the integration of heterostructures because of the weak van der Waals interaction between different layers without dangling bonds at the interfaces. It is easy to grow 2D materials van der Waals heterostructures as there is no limitation of the constraints of lattice matching and processing compatibility. Various van der Waals heterostructures have been demonstrated, including tunnelling field-effect transistors[1], vertical field-effect transistors[2,3], optoelectronic devices[4,5], light-emitting diodes[6,7] and photovoltaic applications[8,9]. Band-structure engineering of ver der Waals heterostructures is attractive and essential to design and create devices[6,10,11]. One band-structure engineering is combining different 2D crystals and changing their number of layers. It can create a designed potential landscape of electron to live and designed band alignments for electron transport and photon-electron interaction. Numerous band structures of van der Waals heterostructure were designed by proximity effect and electrostatic interaction[11] based on the broad choice of 2D materials. To design More-than-Moore devices, which represent new functional diversification of technologies that combines performance and integration not limited to the previous CMOS scaling, novel band structure engineering of van der Waals heterostructures is necessary. Furthermore, the previously reported electric devices exhibit insufficient control of multifunctionality. Multi-band-structure for multifunctional devices are required.

On the other hand, 2D ferroelectric materials with different and strong coulombic interaction on the two side of 2D materials were observed. In-plane spontaneous electrical polarization in atomic-thick SnTe[12] and out-of-plane polarization in $CuInP_2S_6$[13] above room-temperature have been reported. Recently, the so-called III_2-VI_3 compounds[14–16] have been demonstrated to possess both ferroelectric out-of-plane and in-plane polarization at room temperature. The ferroelectric 2D materials provide platforms for tuning electric properties in van der Waals materials.[17,18].

Here, we propose a novel strategy for band-structure engineering of van der Waals heterostructures using ferroelectric layers. By placing ferroelectric layers (In_2Se_3) on the top and on the bottom of van der Waals semiconducting bilayer CrI_3 (forming a FE/SB/FE sandwich structure), four electronic states with different spin-splitting can be achieved by switching the polarization of the ferroelectric layers, forming an electric-field tunable and non-volatile four-state spin-field effect transistor. In two of these states, spin-splitting conduction band with opposite spin channel is generated by the electric field.

II. METHODS

We perform calculations within the framework of density functional theory (DFT)[19], as implemented in the Vienna *ab-initio* Simulation Package (VASP)[20]. The exchange and correlation functionals are treated within the generalized gradient approximation in the form of Perdew, Burke, and Ernzerhof (PBE) functional[21]. The strong onsite Coulomb interaction on the Cr 3d orbitals was considered by including an effective Hubbard U pa-

rameter of 3.7 eV for Cr (see Fig. S4 in the Supplemental Material to explain this choice for the U value). The electron-ion interaction was described by means of projector augmented wave with $5s^25p^1$, $4s^24p^4$, $3d^5s^1$, and $5s^25p^5$ as valence electrons for In, Se, Cr, and I atoms, respectively. The electronic wave functions were expanded in a plane-wave basis set with a cutoff energy of 400 eV for all cases. For the hexagonal lattices, the lattice vectors are defined as $\mathbf{a} = \frac{1}{2}a_0(\hat{x} - \sqrt{3}\hat{y})$, $\mathbf{b} = \frac{1}{2}a_0(\hat{x} + \sqrt{3}\hat{y})$, and $\mathbf{c} = c_0\hat{z}$, where $\hat{x}$, y, and $\hat{z}$ are the unit vectors along the pseudocubic [100], [010], and [001] direction, respectively. a_0 and c_0 are the in-plane and out-of-plane lattice constants, respectively. A vacuum space of 12 Å was adopted for all calculations, which is thick enough to eliminate the coupling between periodic layers. The van der Waals interaction was described by the optPBE-vdW functional, as proposed in Refs.[22,23]. Structural and atomic relaxations were carried out until the force on each atom was less than 0.001 eVÅ^{-1} while the energy convergence criteria of 10^{-7} eV was adopted. The primitive unit cell and a Γ-centered 6×6×1 k-mesh were used. For the band structure calculations with and without spin-orbit coupling (SOC) as well as by the HSE06 method[24], high-symmetry points K (1/3, 1/3, 0), Γ (0, 0, 0), and M (1/2, 0, 0) were considered.

III. RESULTS

Let us first consider pure two-dimensional In_2Se_3 and CrI_3. The single layer In_2Se_3 has a hexagonal structure with a lattice constant of 4.1 Å. Our calculations predict that it is ferroelectric with an out-of-plane polarization of 2.6 $\mu C/cm^2$, which agrees very well with previous measurements and calculations[14,16,25]. Note that the out-of-plane polarization has been experimentally shown to be easily reversible by an out-of-plane electric field[15,16]. The band structure calculations show a direct band gap of 0.77 eV (which is usually underestimated by DFT calculations) with a valence band maximum (VBM) mainly made of Se p orbitals and a conduction band minimum (CBM) mainly contributed by In s and Se p orbitals (see Fig. S1). The single layer CrI_3 structure is numerically found to have a lattice constant of 7.1 Å, which matches the lattice of In_2Se_3 very well ($4.1 \times \sqrt{3}$) and the heterojunction between In_2Se_3 and CrI_3 is practicably feasible without strain[14,26,27]. Our calculations further present that single layer CrI_3 is a ferromagnetic semiconductor with a band gap of 0.97 eV and about 3 μ_B of magnetic moments on each Cr ion. The VBM for CrI_3 mainly comes from I p orbitals and its CBM mainly originates from Cr t_{2g} orbitals. Very interestingly, both VBM and CBM states near the Fermi level belong to the same spin channel (spin up or spin down) (see Fig. S1). For CrI_3 *bilayer*, it has an antiferromagnetically coupled inter-layers and ferromagnetically coupled intra-layer, forming a A-type ferromagnetism. Therefore, spin-up and spin-down channel levels in bilayer CrI_3 are degenerate in band

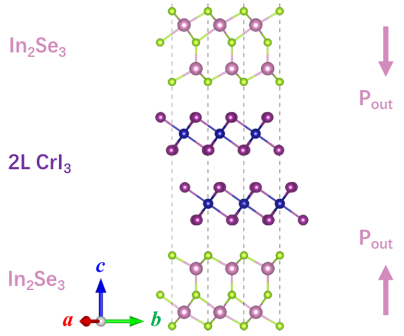

FIG. 1. Ferroelectric clamped sandwich structure of 2D In_2Se_3/bi-CrI_3/In_2Se_3. The out-of-plane directions of ferroelectric polarization in In_2Se_3 layer are indicated by two thick pink arrows.

structure.

As the lattice constants of CrI_3 (a=7.1 Å) and In_2Se_3 ($\sqrt{3}$a=7.1 Å) match very well, the heterostructure between CrI_3 and In_2Se_3 can be easily modeled in one supercell. As shown in Fig. 1, a 2D In_2Se_3/bi-CrI_3/In_2Se_3 heterostructure is made by sandwiching a bilayer A-type AFM CrI_3 compound between two In_2Se_3 monolayers. Different stacking orders between In_2Se_3 and CrI_3, as well as between CrI_3 and CrI_3, are considered. We found that the stacking order between In_2Se_3 and CrI_3 with Cr on the top of Se is the most robust, and Cr ions on top of I ions is the energetically stable in bilayer CrI_3 (see details in Fig. S2 and Table SI in the supplementary materials). The AB2 stacking order of the CrI_3 bilayer with an A-type interlayer antiferromagnetic coupling is one of the most energetically favorable states, as consistent with measurements[28–32]. We will then consider the A-type antiferromagnetic CrI_3 layers in our main text (when clamped by the ferroelectric In_2Se_3 layers, the CrI_3 bilayer also favors the AB2 stacking with an A-type antiferromagnetic order, as shown in Fig. S8). Note that the out-of-plane polarization and in-plane polarization are intrinsically coupled to each other since the reversal of the out-of-plane polarization can also lead to the switching of the in-plane polarization[16]. In our calculations, since the in-plane polarization has a very small effect on the properties of the heterostructure, we mainly study the effect of out-of-polarization on electronic properties.

Based on the directions of the out-of-plane polarizations in the top and bottom In_2Se_3 monolayers of the In_2Se_3/bi-CrI_3/In_2Se_3 heterostructure, there are four structural states (see Fig. 2a): (1) the P1 state that possesses a downward polarization in the top In_2Se_3 layer and upward polarization in the bottom layer (down-up configuration); (2) the P2 state that has an upward polarization in both the top and bottom layers (up-up configuration); (3) the P3 state that adopts a downward polarization in both the top and bottom In_2Se_3 layers (down-down configuration); and (4) the P4 state that exhibits an upward polarization in the top ferroelectric

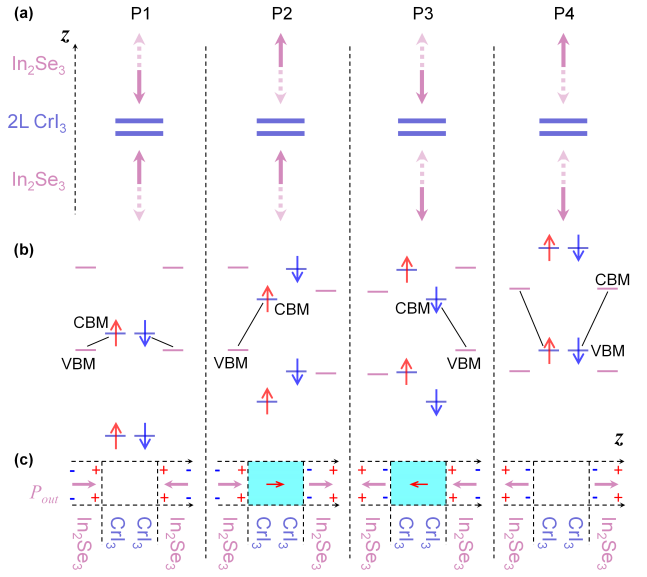

FIG. 2. (a) Schematizations of four states (i.e., P1, P2, P3, and P4), (b) the corresponding band alignments and (c) the sketchs of effective charges as well as effective electric field of of In_2Se_3/bi-CrI_3/In_2Se_3. The directions of out-of-plane polarization in the In_2Se_3 layers are indicated by two thick pink arrows in panel (a). The translucent arrows represent the reversal directions of the polarization components in the In_2Se_3 layers. The red and blue arrows in panel (b) represent the spin up and spin down channel energy level. In panel (c), red "+" and blue "-" represent the positive and negative charges which originates from the our-of-plane polarization, respectively. The cyan region and the small red arrows in P2 and P3 in panel (c) represent the effective built-in electric fields and their directions.

layer and a downward polarization in the bottom ferroelectric In_2Se_3 layer. The schematizations of these four heterostructure states are shown in Fig. 2(a), where the solid thick pink arrows indicate the directions of the polarization of the In_2Se_3 layers while the translucent pink arrows show the opposite directions of polarization that can be switched to from the direction of solid pink arrows. Note that the switching of polarization in In_2Se_3 was confirmed experimentally[15,16] and by some calculations[14,25]. Therefore, these four configurations can be easily switched to one another by two specific electric fields, as shown in Fig. 4. The voltage V_A shown in Fig. 4 is used to control the polarization of top In_2Se_3 and the voltage V_B is used to control the polarization of bottom In_2Se_3 (the doped CrI_3 is supposed to transport carriers very well here for applying voltage).

TABLE I. The shift of band energy level $\Delta\epsilon$ for the two layer CrI_3 (which is calculated by comparing with the vacuum level), band gap E_{gap}, and the spin splitting band situation for the four states of the studied 2D In_2Se_3/bi-CrI_3/In_2Se_3 heterostructure. $\uparrow$ and $\downarrow$ refer to the spin-up and spin-down conduction band near the Fermi level, respectively.

		bi-CrI_3	P1	P2	P3	P4
$\Delta\epsilon$ (eV)	upper CrI_3	0	-1.07	-0.25	0.02	1.01
	lower CrI_3	0	-1.07	0.02	-0.23	1.01
E_{gap} (eV)		0.97	0.14	0.39	0.39	0.58
Spin splitting		–	–	$\uparrow$	$\downarrow$	–

The four configurations of In_2Se_3/bi-CrI_3/In_2Se_3 show very different and interesting electronic structures. As displayed in Fig. 2, in the down-up polarization configuration of P1, there are effective positive charges in the In_2Se_3 layers close to CrI_3 and effective negative charges in the surfaces of top and bottom In_2Se_3 ("+" and "-" in Fig. 2c represent positive and negative charges). Note that these effective charges originates from the polarization in the In_2Se_3 layers. In order to respond to the creation of effective positive charges in In_2Se_3 layers, negative charges are generated in CrI_3 very near the interface with In_2Se_3 (see Fig. S7 of the SM). Such response partly compensates the aforementioned positive charges, but fail in providing a full screening. Under the resulting electrostatic potential, the energy level of both CrI_3 layers shift downward by 1.07 eV, comparing with the pure bilayer CrI_3 (as shown in Table I). As shown in Fig. 2b and Fig. 3a, such downward shift leads to the decrease of the CBM of the system and then results in a reduced band gap of about 0.14 eV. The CBM of Phase I is degenerated between spin-up and spin-down channels, where the spin-up state come from upper CrI_3 layer and spin-down states is from lower CrI_3. (see Figs. 2a and 3a). The VBM of Phase 1 comes from the top and bottom In_2Se_3 layers, belonging to staggered-gap (type II) vdW heterojunction[33,34]. In contrast to P1, the P4 up-down polarization configuration yields a polarization-induced effective negative charges in the In_2Se_3 layers close to the CrI_3 layers (see "-" and "+" in Fig. 2c)and resulting screening-induced effective positive charges located in the CrI_3 layers near the interface with In_2Se_3 (which do not fully screen the effective negative charges because of the semiconducting nature of CrI_3 as hinted by Fig. S7 of the SM). The resulting electrostatic poten-

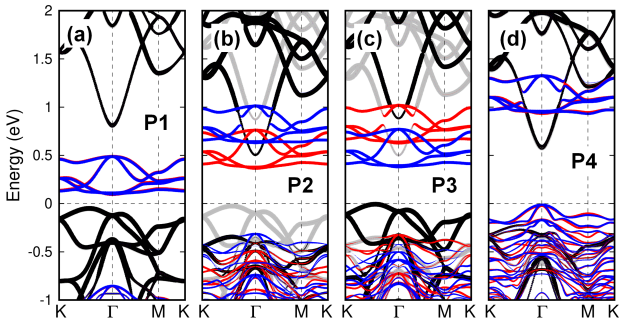

FIG. 3. Projected band structures for the four states of the studied 2D In_2Se_3/bi-CrI_3/In_2Se_3 heterostructure. The black and gray bands represent the bands of top and bottom In_2Se_3 layers, respectively, while the red and blue bands display the spin-up and spin-down bands of bilayer CrI_3, respectively.

tial leads to all band energy levels of CrI_3 increasing by 1.01 eV (see $\Delta\epsilon$ in Table I), resulting in the CBM and VBM of CrI_3 being higher than the CBM and VBM of In_2Se_3, respectively (see Figs. 2b and 3d). The VBM of the heterostructure is then associated with CrI_3 while the CBM lies in the In_2Se_3 layers, in contrast with P1 where the VBM is located at the In_2Se_3 layers and the CBM is acting in the CrI_3 layers (see Figs. 2b, 3a and 3d). The resulting band gap is now 0.58 eV, which is much larger than the one of P1. The difference in band gap and difference in character of the VBM and CBM (between CrI_3 and In_2Se_3 layers) in P1 and P4 states may induce sharp different transport properties, when going from P1 to P4 and conversely (in that sense such transition can provide an on-off control in transistors).

Let us now investigate the electronic properties of P2 and P3. For P2, since the out-of-plane polarization in both the top and bottom In_2Se_3 layers is upwards, there are effective negative (positive) charges in the top (bottom) In_2Se_3 layer close to the CrI_3 bilayers. There is a built-in effective electric field between the top and bottom In_2Se_3 layers along the upwards direction (see Fig. 2c). Under this effective electric field, the bands energy of the upper CrI_3 layer shift to higher energy, while the bands energy of the lower CrI_3 layer shifts to lower energy. This shift leads to about 0.25 eV difference between the band structures of two CrI_3 layer, which different from P1 and P4 for which the band energy is same for the two middle CrI_3 layers. This shift of energy levels also results in a spin-splitting of band structure in the bilayer CrI_3. The conduction bands near the Fermi level belong to spin-up channel associated with the lower CrI_3 layer. This should lead to only spin-up current in transport devices! Note that the two spins are degenerate in *pure* bilayer CrI_3 layers because of the A-type antiferromagnetic configuration (see Fig. S1). Spin splitting band structure in the In_2Se_3/bi-CrI_3/In_2Se_3 sandwich structure is generated by a magnetoelectric effect from spin degenerated band structure of pure bilayer CrI_3. In contrast, in P3, the out-of-plane polarizations in the top and bottom In_2Se_3 layers are both downwards and an effective build-in electric field along the downward direction is then created. Under this electric field, the band energy of the upper CrI_3 layer shifts downwards while the band energy of the lower CrI_3 layer shifts upwards as compared with pristine CrI_3. The shift of the band structure in P3 state leads to same band gap as P2, but to different CBM than P2. As a matter of fact, the CBM of P3 is a spin-down channel contributed by the upper CrI_3 layer while it is a spin-up channel located by lower CrI_3 layer for P2 (see Fig. 2 and 3). The band structure of P3 can thus provide spin-down spin current in transport devices. These electronic structure in P2 and P3 are very interesting, since they provide a tunable spin-field effect transistor where one type of spin current can be switched to another type of spin current by an electric-field-induced transformation from the P2 to P3 configurations.

Figure 4 represents a schematic in a device for which

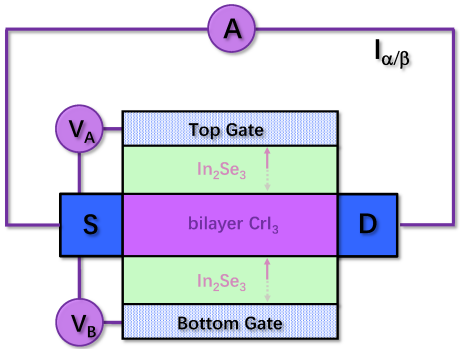

FIG. 4. Schematic structure of the designed 2D semiconductor spin-field effect transistor based on the 2D In_2Se_3/bi-CrI_3/In_2Se_3 heterostructure. The source (S) and drain (D) are ferromagnetic metal. The gate voltage V_A and V_B are applied to switch the polarization of In_2Se_3 layers and control the states of the system.

the polarizations in the top and bottom ferroelectric layers can be easily switched by two different voltages. V_A generates an electric field between the top gate and the bi-CrI_3 layers (we suppose that a doped semiconductor of bilayer CrI_3 can transport carriers very well here). As a result the polarization of the top In_2Se_3 layer can be switched by V_A. Furthermore, V_B generates an electric field between the bottom gate and the bi-CrI_3 layer, which can switch the polarization of the bottom In_2Se_3 layer. Therefore, the four phases in In_2Se_3/bi-CrI_3/In_2Se_3 shown in Fig. 1 can be easily switched to one other. P1 and P4 are two spin degenerated states of field effect transistors with different band gaps, P2 and P3 are spin-splitting states with different spin-channels in the conduction band. We thus propose a new spin-field effect transistor with four tunable states. Note also that ohmic contacts between source-CrI_3 and drain-CrI_3 are necessary for spin electric field effect device. As compared with the suggested spin-field effect transistor made by two layers of VSe_2 under electric field[35] or dual-gated graphene/CrI_3/graphene[36],the presently designed spin-field effect transistor not only has four tunable states but is also nonvolatile, therefore making the device more powerful, functional, practical and energy saving.

Moreover, Table I shows the shift of band energy of the CrI_3 layers and the band gap of the heterostructure in the four phases. The band gap E_{gap} and the shift of band energy level $\Delta\epsilon$ may slightly change under the strain arising from substrate[37]. Note that the value of the band shift and band gap can be further tuned using ferroelectric layers with different magnitude of polarization. Thanks to the development of two-dimensional materials, various two-dimensional ferroelectrics are synthesized or cleaved, such as monolayer d1T-$MoTe_2$[38], $CuInP_2S_6$ ultrathin flakes[13], and even layered oxides, such as $YMnO_3$[39], $LuFeO_3$[40]. Therefore, placing the two-dimensional ferroelectric materials with different magnitude of polarization on the top and bottom of van der

Waals heterostructure, $\Delta\epsilon$ and E_{gap} in Table I can be further changed and even continuously tuned because continuously changed magnitude of ferroelectric polarization can be used.

IV. CONCLUSIONS

In summary, we propose a new band structure engineering for van der Waals heterostructure from first principles. Two-dimensional ferroelectric (FE) layers were placed on top and bottom of a semiconducting bilayer (SB) to tune its band structure. This sandwich structure of FE/SB/FE then has four states with different band gaps and spin-splitting electronic band structures, thus forming a novel electric controllable and non-volatile four-state spin-field effect transistor. Furthermore, the FE and SB in the sandwich structure can be any ferroelectric layer with out-of-plane polarization and A-AFM semiconducting bilayer, respectively. Band gaps can be even continuously tuned using ferroelectric layers with different magnitude of polarization. As the various 2D ferroelectric and A-AFM semiconducting structures, the proposed band-structure engineering of van der Waals heterostructure represents an appealing and diverse route for modern electronics and spintronics.

ACKNOWLEDGMENTS

Y.Y and H.T. thank for NSFC (Contract No. 11874207) and National Key R&D Program of China (Grant No. 2020YFA0711504). L.B. acknowledges ONR Grant No. N00014-17-1-2818. H.T. also thanks he support of the China Postdoctoral Science Foundation (No. 2018M642205) and the Jiangsu Planned Projects for Postdoctoral Research Funds (No. 2019K249). We are grateful to the HPCC resources of Nanjing University for the calculations.

* yangyr@nju.edu.cn(Y. Yang)
† diwu@nju.edu.cn(D. Wu)

[1] L. Britnell, R. Gorbachev, R. Jalil, B. Belle, F. Schedin, A. Mishchenko, T. Georgiou, M. Katsnelson, L. Eaves, S. Morozov, *et al.*, Science **335**, 947 (2012).
[2] T. Georgiou, R. Jalil, B. D. Belle, L. Britnell, R. V. Gorbachev, S. V. Morozov, Y.-J. Kim, A. Gholinia, S. J. Haigh, O. Makarovsky, *et al.*, Nat. Nanotechnol. **8**, 100 (2013).
[3] W. J. Yu, Z. Li, H. Zhou, Y. Chen, Y. Wang, Y. Huang, and X. Duan, Nat. Mater. **12**, 246 (2013).
[4] L. Britnell, R. Ribeiro, A. Eckmann, R. Jalil, B. Belle, A. Mishchenko, Y.-J. Kim, R. Gorbachev, T. Georgiou, S. Morozov, *et al.*, Science **340**, 1311 (2013).
[5] C.-H. Lee, G.-H. Lee, A. M. Van Der Zande, W. Chen, Y. Li, M. Han, X. Cui, G. Arefe, C. Nuckolls, T. F. Heinz, *et al.*, Nat. Nanotechnol. **9**, 676 (2014).
[6] F. Withers, O. Del Pozo-Zamudio, A. Mishchenko, A. Rooney, A. Gholinia, K. Watanabe, T. Taniguchi, S. Haigh, A. Geim, A. Tartakovskii, *et al.*, Nat. Mater. **14**, 301 (2015).
[7] F. Xia, H. Wang, D. Xiao, M. Dubey, and A. Ramasubramaniam, Nat. Photonics **8**, 899 (2014).
[8] Y. Xue, Y. Zhang, Y. Liu, H. Liu, J. Song, J. Sophia, J. Liu, Z. Xu, Q. Xu, Z. Wang, *et al.*, ACS Nano **10**, 573 (2016).
[9] N. Flöry, A. Jain, P. Bharadwaj, M. Parzefall, T. Taniguchi, K. Watanabe, and L. Novotny, Appl. Phys. Lett. **107**, 123106 (2015).
[10] A. K. Geim and I. V. Grigorieva, Nature **499**, 419 (2013).
[11] K. Novoselov, A. Mishchenko, A. Carvalho, and A. C. Neto, Science **353**, aac9439 (2016).
[12] K. Chang, J. Liu, H. Lin, N. Wang, K. Zhao, A. Zhang, F. Jin, Y. Zhong, X. Hu, W. Duan, Q. Zhang, L. Fu, Q.-K. Xue, X. Chen, and S.-H. Ji, Science **353**, 274 (2016).
[13] A. Belianinov, Q. He, A. Dziaugys, P. Maksymovych, E. Eliseev, A. Borisevich, A. Morozovska, J. Banys, Y. Vysochanskii, and S. V. Kalinin, Nano Lett. **15**, 3808 (2015).
[14] W. Ding, J. Zhu, Z. Wang, Y. Gao, D. Xiao, Y. Gu, Z. Zhang, and W. Zhu, Nat. Commun. **8**, 14956 (2017).
[15] Y. Zhou, D. Wu, Y. Zhu, Y. Cho, Q. He, X. Yang, K. Herrera, Z. Chu, Y. Han, M. C. Downer, H. Peng, and K. Lai, Nano Lett. **17**, 5508 (2017).
[16] C. Cui, W.-J. Hu, X. Yan, C. Addiego, W. Gao, Y. Wang, Z. Wang, L. Li, Y. Cheng, P. Li, X. Zhang, H. N. Alshareef, T. Wu, W. Zhu, X. Pan, and L.-J. Li, Nano Lett. **18**, 1253 (2018).
[17] M. Gibertini, M. Koperski, A. F. Morpurgo, and K. S. Novoselov, Nat. Nanotechnol. **14**, 408 (2019).
[18] C. Gong and X. Zhang, Science **363**, eaav4450 (2019).
[19] W. Kohn and L. J. Sham, Phys. Rev. **140**, A1133 (1965).
[20] G. Kresse and J. Furthmüller, Phys. Rev. B **54**, 11169 (1996).
[21] J. P. Perdew, K. Burke, and M. Ernzerhof, Phys. Rev. Lett. **77**, 3865 (1996).
[22] J. Klimeš, D. R. Bowler, and A. Michaelides, J. Phys.: Condens. Matter **22**, 022201 (2009).
[23] J. c. v. Klimeš, D. R. Bowler, and A. Michaelides, Phys. Rev. B **83**, 195131 (2011).
[24] A. V. Krukau, O. A. Vydrov, A. F. Izmaylov, and G. E. Scuseria, J. Chem. Phys **125**, 224106 (2006).
[25] X. Jiang, Y. Feng, K.-Q. Chen, and L.-M. Tang, J. Phys.: Condens. Matter **32**, 105501.
[26] C. Gong, E. M. Kim, Y. Wang, G. Lee, and X. Zhang, Nat. Commun. **10**, 2657 (2019).
[27] C. Xu, J. Feng, H. Xiang, and L. Bellaiche, npj Comput. Mater. **4**, 57 (2018).
[28] B. Huang, G. Clark, D. R. Klein, D. MacNeill, E. Navarro-Moratalla, K. L. Seyler, N. Wilson, M. A. McGuire, D. H. Cobden, D. Xiao, *et al.*, Nat. Nanotechnol. **13**, 544 (2018).
[29] S. Jiang, L. Li, Z. Wang, K. F. Mak, and J. Shan, Nat. Nanotechnol. **13**, 549 (2018).

[30] N. Sivadas, S. Okamoto, X. Xu, C. J. Fennie, and D. Xiao, Nano Lett. **18**, 7658 (2018).
[31] P. Jiang, C. Wang, D. Chen, Z. Zhong, Z. Yuan, Z.-Y. Lu, and W. Ji, Phys. Rev. B **99**, 144401 (2019).
[32] Y. Lu, R. Fei, X. Lu, L. Zhu, L. Wang, and L. Yang, ACS Appl. Mater. Interfaces **12**, 6243 (2020).
[33] R. Marschall, Adv. Funct. Mater. **24**, 2421 (2014).
[34] M. Mikhailova, K. Moiseev, T. Voronina, T. Lagunova, and Y. P. Yakovlev, Semiconductors **41**, 161 (2007).
[35] S.-J. Gong, C. Gong, Y.-Y. Sun, W.-Y. Tong, C.-G. Duan, J.-H. Chu, and X. Zhang, Proc. Natl. Acad. Sci. U.S.A. **115**, 8511 (2018).
[36] S. Jiang, L. Li, Z. Wang, J. Shan, and K. F. Mak, Nat. Electron. **2**, 159 (2019).
[37] P. Hou, Y. Lv, Y. Chen, Y. Liu, C. Wang, P. Zhou, X. Zhong, J. Wang, and X. Ouyang, ACS Appl. Electron. Mater. **2**, 140 (2019).
[38] S. Yuan, X. Luo, H. L. Chan, C. Xiao, Y. Dai, M. Xie, and J. Hao, Nat. Commun. **10**, 1775 (2019).
[39] W. Wang, J. Zhao, W. Wang, Z. Gai, N. Balke, M. Chi, H. N. Lee, W. Tian, L. Zhu, X. Cheng, D. J. Keavney, J. Yi, T. Z. Ward, P. C. Snijders, H. M. Christen, W. Wu, J. Shen, and X. Xu, Phys. Rev. Lett. **110**, 237601 (2013).
[40] M. Lilienblum, T. Lottermoser, S. Manz, S. M. Selbach, A. Cano, and M. Fiebig, Nat. Phys. **11**, 1070 (2015).